JOURNAL OF CATALYSIS **161,** 626–640 (1996)
ARTICLE NO. 0225

Characterization of Carbonaceous Species Formed during Reforming of CH_4 with CO_2 over Ni/CaO–Al_2O_3 Catalysts Studied by Various Transient Techniques

M. A. Goula,* A. A. Lemonidou,* and A. M. Efstathiou†,[1]

*Chemical Process Engineering Research Institute, CPERI-FORTH, and Department of Chemical Engineering, Aristotle University of Thessaloniki, P.O. Box 1517, Thessaloniki 54006; and †Institute of Chemical Engineering and High Temperature Chemical Processes, ICE/HT-FORTH, P.O. Box 1414, University Campus, Patras GR-26500, Greece

Received August 1, 1995; revised January 31, 1996; accepted February 12, 1996

Carbon dioxide reforming of methane to synthesis gas at 750°C over 5 wt% Ni/CaO–Al_2O_3 catalysts has been investigated with respect to effects of support composition (CaO to Al_2O_3 ratio) on catalyst stability, amount and reactivity of carbon species formed during reaction, and relative proportion of reaction routes that lead to carbon formation (CH_4 vs CO_2 molecule). Temperature-programmed oxidation (TPO) and hydrogenation (TPH) experiments, following reforming reaction with 20% CH_4/20% CO_2/He and 20% $^{13}CH_4$/20% CO_2/He mixtures, have been conducted for the aforementioned carbon characterization studies. Two kinds of carbon species (free of chemically bound hydrogen) were mainly found to accumulate on the catalyst surface, where the amount and reactivity of them are influenced by the CaO/Al_2O_3 ratio used to deposit the nickel metal. Transient isothermal hydrogenation experiments of the carbon species formed during reforming reaction resulted in CH_4 responses, where the time of appearance of the CH_4 peak maximum in hydrogen stream as a function of hydrogenation temperature was used to obtain the intrinsic activation energy of the hydrogenation process. It was found that this activation energy is influenced by the support composition. TPO experiments conducted following reforming reaction with $^{13}CH_4/CO_2$/He mixture have demonstrated that the relative amount of adsorbed carbon species formed via the CH_4 and CO_2 molecular routes was strongly dependent on support composition. H_2 temperature-programmed desorption, temperature-programmed reduction, and X-ray photoelectron spectroscopic measurements conducted over the present catalysts suggest that the nickel particle morphology and its size distribution must be influenced by the support composition, which in turn controls the origin, the kinetics, and the reactivity of carbon deposition under reforming reaction conditions.

INTRODUCTION

There is a growing interest in the process of carbon dioxide reforming of methane to synthesis gas which results in a suitable CO/H_2 ratio for the production of higher hydrocarbons and oxygenated derivatives. This reaction is slightly more endothermic than the steam reforming of methane, the latter being a well-established industrial process for producing synthesis gas rich in hydrogen appropriate for the synthesis of methanol (1, 2). Supported noble metals have shown higher activity and lower sensitivity to coking than other supported metal and metal oxide catalysts (3–8). However, the fact that these noble metals are high in cost and limited in availability makes the development of nickel-based catalysts for appropriate industrial practice a challenge to the catalytic scientific community.

There is a limited amount of fundamental research concerning the reforming of CH_4 with CO_2 over nickel-based catalysts, where most of the research work concerns the examination of catalytic activity and stability with time on stream (3, 7, 9–17). Gadalla and Sommer (11) have shown that over supported nickel catalysts, deactivation is due to either carbon deposition, metal sintering, or phase transformation, such as the formation of $NiAl_2O_4$ in the case of a Ni/γ-Al_2O_3 catalyst. All these phenomena, however, depend on reaction conditions (temperature, CH_4/CO_2 ratio) and the calcination temperature used during and after preparation of the catalyst. Zhang and Verykios (10) have recently shown that the stability of a 17 wt% Ni/γ-Al_2O_3 catalyst was improved by the addition of CaO (CaO/$Al_2O_3 = 1/9$) in the support composition. Temperature-programmed oxidation experiments performed following reforming reaction have indicated that the reactivity toward oxidation to CO_2 of the carbon species formed during reforming reaction increased in the case of a CaO-promoted catalyst as compared with a Ni/γ-Al_2O_3 catalyst. It was suggested (10) that the improved stability of the CaO-promoted catalyst may be related to the enhanced reactivity of carbon formed under reforming reaction conditions and, thus, to the lower amount of accumulated carbon. Similarly, Ruckenstein and Hu (15) have observed high stability and activity over a reduced 20 wt% NiO/MgO catalyst as compared with NiO/CaO, Ni/SrO, and

[1] To whom correspondence should be addressed. Fax: +(3061)-993.255.

0021-9517/96 $18.00

Ni/BaO catalysts due to the formation of NiO–MgO solid solution which suppressed carbon accumulation.

Osaki *et al.* (14) have recently studied the effect of support composition on the reactivity and chemical structure of CH_x adsorbed species, the latter suggested to arise from the CH_4 decomposition step during reforming of CH_4 with CO_2 over supported Ni catalysts. In particular, the intrinsic reactivity (k, s^{-1}) of the CH_x species associated with the elementary reaction step $CH_{x,ads} + O_{ads} \leftrightharpoons CO_{ads} + xH_{ads}$ was found to be influenced by the support composition. In the present study, a support effect on the reactivity of carbon species toward oxidation and hydrogenation, the latter species formed during reforming reaction at 750°C, was also evident over 5 wt% Ni/CaO–Al_2O_3 catalysts with different CaO/Al_2O_3 molar ratios in support composition.

It is well known that deactivation of supported Ni catalysts in steam reforming of methane is due mainly to carbon deposition, which poisons the nickel active surface and further causes blockage of pore mouths of the catalyst support and even its physical disintegration (18). Fundamental knowledge concerning the coking process is, therefore, required to improve the resistance to coking of a nickel-based catalyst for the reforming of CH_4 with CO_2 to a degree acceptable for industrial application. In particular, the following basic questions related to this aspect need to be answered:

- How does carbon deposition influence the stability of the catalyst?
- How do nickel-support interactions affect the kind of deposited carbon and its reactivity?
- What is the individual role of CH_4 and CO_2 reaction pathways in the accumulation of adsorbed carbon under reforming reaction conditions?
- What are the chemical and morphological properties of the carbon species formed?

This work is focused on the investigation of fundamental aspects of the coking process occurring over Ni/CaO–Al_2O_3 catalysts during reforming of methane with carbon dioxide at 750°C. Attempts are made to answer some of the questions mentioned above which concern the coking process by employing various transient methods with on-line mass spectrometry. Measurements of accumulated carbon under reforming reaction conditions which is specifically derived from the CH_4 or CO_2 molecules was done by replacing $^{12}CH_4$ with $^{13}CH_4$ isotope gas in the feedstream.

EXPERIMENTAL

A. Catalyst Preparation and Characterization

The carriers employed for the preparation of supported nickel catalysts were mechanical mixtures of $CaCO_3$ (J. T. Baker, Analyzed Reagent) and γ-Al_2O_3 (Catapal alumina, calcined at 650°C for 2 h) calcined at 1100°C. Mixtures of CaO/Al_2O_3 at molar ratio of 1/2 and 12/7 were used in this work. The resulting calcium aluminate supports were found to have a mean particle size of 300 μm. Details of the preparation and calcination procedures of the carriers employed can be found elsewhere (19). Catalysts were prepared by the method of incipient wetness impregnation using an aqueous solution of nickel nitrate so as to yield 5 wt% metal loading. The resulting material was then dried and heated in an oven for 4 h at 600°C. It was subsequently calcined in air for 10 h at 900°C, cooled slowly to ambient conditions, and stored until further use. For catalytic and transient studies, different fresh samples have been used which were first reduced in H_2 at 750°C for 1 h.

The BET surface area of the catalyst samples was measured using a Micromeritics Accusorb 2100E instrument with nitrogen as the adsorbate gas. Metal dispersion of fresh catalyst samples, following H_2 reduction at 750°C for 2 h, was measured by H_2 chemisorption followed by temperature-programmed desorption (TPD) as presented under Results. The accumulation of carbonaceous species on the catalyst surface as a function of time on stream and their reactivity toward oxidation and hydrogenation were studied by temperature-programmed oxidation (TPO) and hydrogenation (TPH) methods, respectively. Transient isothermal hydrogenation experiments of carbonaceous species have also been conducted to obtain kinetic information concerning the hydrogenation process. These experiments, and those of TPO, TPH, and H_2 chemisorption/TPD mentioned above, were performed in a specially designed flow system for transient studies, details of which have been given elsewhere (20). The amount of carbon deposited on the catalyst surface during reforming reaction for long times on stream (18 h) was determined using a CHN analyzer (LECO).

A Siemens D500 X-ray diffractometer was used to identify the crystalline phases of supported nickel catalysts. The adsorbed species formed on the working catalyst surface at 700°C were investigated by *in situ* Fourier transform infrared (FT-IR) spectroscopy (Perkin Elmer 1710 spectrometer) employing a diffuse reflectance cell. X-ray photoelectron spectroscopy (XPS) was used for surface analysis and characterization employing a Leybold LHS 10 spectrometer equipped with a single channel detector coupled with an Al $K\alpha$ radiation source (power settings: 12 kV × 23 mA). The analyzer was used in the pass energy mode with a PE of 100 eV. Each powdered sample was pressed into a pellet and mounted on the sample probe; the latter was placed in a preevacuation chamber ($\sim 10^{-5}$ Torr), before it was moved into the main vacuum chamber ($< 7 \times 10^{-9}$ Torr). Each spectral region was signal-averaged for a given number of scans to obtain a good signal-to-noise ratio. Although surface charging was observed on all samples, accurate binding energies were determined by charge referencing to the Ca ($2p^{3/2}$) line of 347 eV. Peak areas were computed by software

that used Gaussian peak shapes and flat background subtraction. Atomic surface concentrations were calculated based on well-established relationships (21), where appropriate atomic sensitivity factors have been used (21).

B. Catalyst Testing

Activity measurements were conducted at 1 atm in a conventional flow apparatus consisting of a flow measuring and control system, a mixing chamber, a quartz fixed bed reactor, and an on-line gas chromatograph. The quartz reactor (i.d. = 9 mm) was electrically heated by a furnace with three independently heated zones, while the temperature profile was measured using a chromel–alumel thermocouple placed in an axial thermowell centered in the catalyst bed. The reaction products were analyzed using a Varian 3700 gas chromatograph equipped with a TC detector. Two columns, Poropak Q and Molecular Sieve 5A, were used in a series/bypass arrangement for the complete separation of H_2, O_2, CH_4, CO, and CO_2. The catalysts were reduced in H_2 flow at 750°C for 1 h before testing.

C. Gases

A mixture consisting of 20% $^{13}CH_4$, 20% CO_2, and 60% He was prepared using a lecture bottle of $^{13}CH_4$ which was of 99% ^{13}C content (Isotec Inc.). The H_2 and He gases used in transient studies were standard (99.995%) and ultrahigh purity (99.999%), respectively. Further purification of these gases was performed by using molecular sieve (13X) and MnO_x traps for removing traces of water and oxygen, respectively.

D. Mass Spectrometry

Chemical analysis of the gases during transients was done with an on-line mass spectrometer (Fisons, SXP Elite 300H) equipped with a fast response inlet capillary/leak diaphragm system. Calibration of the mass spectrometer signal was performed based on prepared mixtures of known composition. The output signal from the mass spectrometer detector was then converted to mole fraction, y (mol%), by appropriate software. For the measurement of CO ($m/z = 28$) in the presence of CO_2 ($m/z = 44$) and of ^{13}CO ($m/z = 29$) in the presence of $^{13}CO_2$ ($m/z = 45$), the contribution of CO_2 and $^{13}CO_2$ to the 28 and 29 peaks, respectively, was estimated by feeding a mixture of 1% CO_2/He to the mass spectrometer. Similar measurements were performed to estimate the ratio of 15/30 for the contribution of C_2H_6 ($m/z = 30$) to the $m/z = 15$ signal in the case of a mixture of CH_4 and C_2H_6 gases.

RESULTS

A. Catalyst Characterization

The crystalline phases of Ni/CaO–Al_2O_3 catalysts investigated by X-ray diffraction (XRD) are presented in Table 1 along with their BET surface areas. The XRD results correspond to calcined samples as described under Experimental. Catalyst A ($CaO/Al_2O_3 = 1/2$) consists mainly of NiO, $CaAl_4O_7$, $CaAl_2O_4$, and α-Al_2O_3 phases and of a minor $NiAl_2O_4$ phase. By increasing the CaO/Al_2O_3 ratio from 1/2 to 12/7 (catalyst B), only two crystalline phases have been identified (NiO and $Ca_{12}Al_{14}O_{33}$). Due to some overlapping of the most intense 2θ peaks of NiO with those of calcium aluminates, it was not possible to determine the average crystal size of NiO. It is noted that the calcium aluminate phase identified in catalyst B is different than that in catalyst A. The BET surface area of catalyst A ($CaO/Al_2O_3 = 1/2$) was found to be about 3.5 times larger than that of catalyst B ($CaO/Al_2O_3 = 12/7$) (see Table 1). XRD measurements performed over used catalyst samples (after 18 h of reaction) revealed the same bulk support phases as shown in Table 1. However, the metal is now found to be in the form of Ni crystals instead of NiO (the case of calcined sample).

TABLE 1

Characterization of Ni/CaO–Al_2O_3 Catalysts after Calcination at 900°C

Catalyst designation	Support (mol basis)	Nickel content (wt%)	Surface area (m^2/g)	Crystal phases
A	$1CaO/2Al_2O_3$	5	5.7	NiO, $NiAl_2O_4$[a] $CaAl_4O_7$, $CaAl_2O_4$ α-Al_2O_3
B	$12CaO/7Al_2O_3$	5	1.6	NiO, $Ca_{12}Al_{14}O_{33}$

[a] Minor phase.

The reduction characteristics of the calcined Ni/CaO–Al_2O_3 catalysts were studied as follows: The fresh catalyst sample was first treated with 10% O_2/He at 750°C for 1 h. The feed was then switched to He for 5 min at 750°C, and the reactor was subsequently cooled in He flow to 300°C. The feed was then changed to 1% H_2/He mixture, while the temperature was increased to 750°C at the rate of 30°C/min. The H_2 response was followed by on-line mass spectrometry, and this is shown in Figs. 1a and b, in the case of catalyst A and catalyst B, respectively. On introduction of the H_2/He mixture over the catalyst at 300°C, there is a sharp increase in the H_2 response signal from its background value (under He flow) toward the value corresponding to its feed concentration (1 mol%). However, the latter signal value is not obtained since some very small consumption of H_2 takes place. As the temperature of the reduction process increases, the H_2 gas-phase concentration decreases (passing through a maximum, see Fig. 1), where at about 500°C practically all the hydrogen fed to the reactor is consumed. This result remains the same until the temperature of 750°C is reached

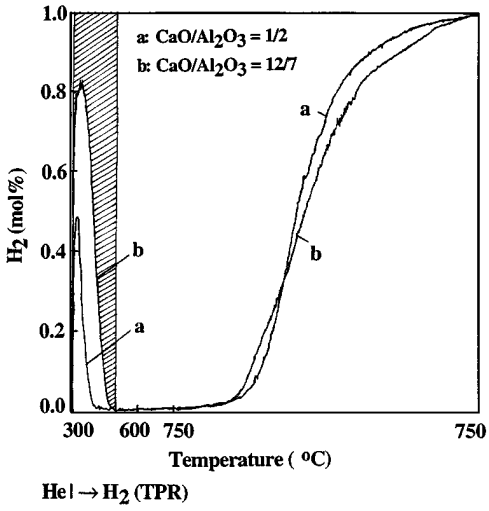

FIG. 1. Hydrogen temperature-programmed reduction (TPR) of calcined 5 wt% Ni/CaO–Al_2O_3 catalysts. Gas delivery sequence: 10% O_2/He (750°C, 1 h) → He (750°C, 5 min) → cool in He flow to 300°C → 1% H_2/He ($\beta = 30$°C/min). $W = 0.5$ g; $Q = 30$ ml/min (ambient). (a) Catalyst A ($CaO/Al_2O_3 = 1/2$); (b) catalyst B ($CaO/Al_2O_3 = 12/7$).

(end of the TPR process). From that point the temperature of the catalyst is held at 750°C for 40 min (catalyst A) and 80 min (catalyst B) until the H_2 response signal takes the value corresponding to its feed concentration (1 mol%). At this point, no further H_2 consumption by the catalyst sample takes place. The shaded area in Fig. 1 is proportional to the amount of H_2 uptake by catalyst B (curve b) in the range 300–500°C. The corresponding hydrogen uptake by catalyst A is given by the sum of the shaded area and that between the two hydrogen response curves, a and b. It is therefore apparent that the degree of reduction of NiO to Ni^0 in the range 300–500°C is larger in the case of catalyst A than of catalyst B. On the other hand, in both cases most of the reduction (~70%) occurs in the range 500–750°C, where the total amount of H_2 consumed is approximately the same for both catalysts (catalyst A: 830 μmol/g; catalyst B: 806 μmol/g).

An estimate of the number of reduced surface nickel atoms in the fresh catalyst samples (before reaction studies) has been attempted by selective hydrogen chemisorption followed by TPD. Figures 2a and b show the hydrogen responses obtained during TPD with catalysts A and B, respectively. The experimental procedure applied was as follows: After reduction of the fresh calcined catalyst sample with pure H_2 at 750°C for 1 h, the reactor was purged in He for 5 min at 750°C and cooled in He flow to 300°C. The feed was then switched to pure H_2 for 15 min, while the catalyst was subsequently cooled in H_2 flow to 30°C and remained at this temperature for $\frac{1}{2}$ h. The feed was then changed to He for 3 min to remove the H_2 from the gas phase of the reactor and the lines, followed by heating of the reactor to 750°C at the rate of 30°C/min. In the case of catalyst A, most of the H_2 desorbs at temperatures lower than 500°C (Fig. 2a), while in the case of catalyst B about 60% of chemisorbed H_2 desorbs at temperatures higher than 500°C (Fig. 2b). In both cases, three H_2 desorption peaks are observed, while a shoulder is developed on the high-temperature side of the third desorption peak. A significant shift toward higher desorption temperatures is obtained in the case of the third hydrogen desorption peak corresponding to catalyst B ($T_{M3} = 540$°C) as compared with that of catalyst A ($T_{M3} = 230$°C).

Comparing the two H_2 TPD spectra shown in Fig. 2, it is seen that in the case of catalyst A the number of sites that desorb H_2 in the range 30–500°C is about three times that corresponding to catalyst B, whereas the total amount of H_2 adsorption is approximately the same for both catalysts. The number of active sites per gram of catalyst with high binding energies of H_2 adsorption (H_2 desorption at $T > 500$°C) is larger in the case of catalyst B than of catalyst A. The amounts of surface reduced Ni sites per gram of catalyst corresponding to the H_2 chemisorption results shown in Fig. 2 are found to be 42.6 and 38.3 μmol/g_{cat} for catalysts A and B, respectively ($H/Ni_s = 1$). These quantities correspond to metal dispersions of 5 and 4.5%, respectively.

XPS measurements have been performed over both fresh catalysts after being calcined at 900°C (see Sect. A under Experimental). It was found that the Ni($2p^{3/2}$) binding energies are 855.3 and 855.7 eV in the case of catalysts A and B, respectively. According to the literature (22, 23), these values are closely related to bulk NiO and $NiAl_2O_4$ phases, in accordance also with the XRD results previously mentioned. By taking the ratio $\alpha = A_{Ni}/(A_{Ca} + A_{Al})$, where A_i is

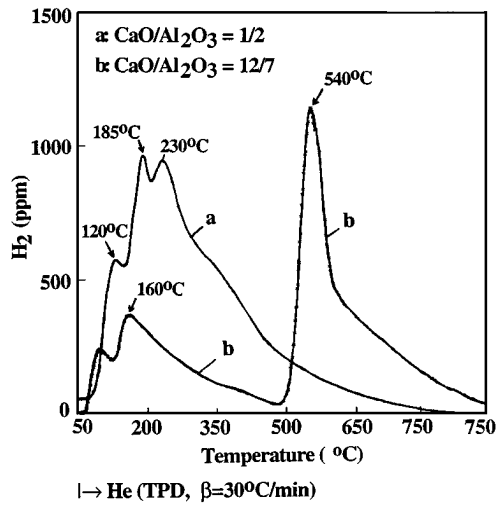

FIG. 2. Hydrogen temperature-programmed desorption (TPD) responses obtained with 5 wt% Ni/CaO–Al_2O_3 catalysts. Gas delivery sequence: H_2 (750°C, 1 h) → He (750°C, 5 min) → cool in He flow to 300°C → H_2 (300°C, 15 min) → cool in H_2 flow to 30°C, stay for 30 min → He (30°C, 3 min) → TPD ($\beta = 30$°C/min). $W = 0.5$ g; $Q = 30$ ml/min (ambient). (a) Catalyst A; (b) Catalyst B.

the area of a given XPS peak, it was found that this ratio was higher on catalyst A than on catalyst B ($\alpha = 1.32$ vs 0.92). Of interest is the surface atomic concentration of oxygen in the two samples, since this parameter could be related to the extent of interactions of Ni^{2+} with surface oxygen ions of support during catalyst preparation and calcination procedures, an issue that is discussed later. Based on the XPS peak areas of O(1*s*), Ni($2p^{3/2}$), Ca($2p^{3/2}$), and Al(2*p*), it was found that the atomic surface oxygen concentration is 0.58 and 0.65 on catalysts A and B, respectively.

B. Catalyst Performance and Stability

Figure 3 shows the alteration of the CH_4 conversion as a function of time on stream at 750°C over the two Ni/CaO–Al_2O_3 catalysts. The methane partial pressure used was 0.2 bar, the CH_4/CO_2 ratio was 1.0, and the *W/F* ratio was 4 kg · s mol^{-1}. As clearly shown in Fig. 3, over a testing period of 18 h there is practically no loss of activity over both catalysts, except in the period of 15–60 min of reaction where drops in CH_4 conversion by 4 and 7 percentage units occur in the case of catalysts A and B, respectively. Similar results have been obtained concerning CO_2 conversion. In the case of catalyst A, the CH_4 conversion obtained after 18 h of reaction (Fig. 3) corresponds to 75% of the equilibrium value, a result that suggests that the catalyst stability is not due to the possibility that part of the catalyst bed may not participate in the reaction; this possibility could exist if the reforming reaction were studied under equilibrium conditions. It is noted that an increase in the *W/F* value corresponding to the results of Fig. 3 would result in equilibrium reaction. For both catalyst formulations, the H_2/CO ratio, the selectivity of CO, S_{CO}, and the hydrogen selectivity, S_{H_2}, are found to be practically the same, namely, 0.94, 100%, and 98%, respectively. The hydrogen selectivity is based on the H_2 and H_2O products formed. These results along with the H_2 and CO yields of reaction are reported in Table 2. Of interest is the fact that despite the small drop in CH_4 and CO_2 conversions observed during the first 1 h of reaction, the hydrogen selectivity of the reaction hardly changed. It was found that by increasing the CaO/Al_2O_3 molar ratio in support composition, the carbon accumulated during 18 h of continuous reaction increases from 3.92 to 7.4 wt%. This result is also reported in Table 2.

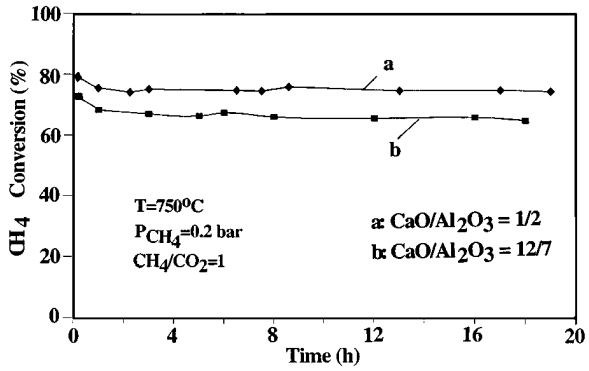

FIG. 3. Variation of the CH_4 conversion with time on stream over 5 wt% Ni/CaO–Al_2O_3 catalysts. $T = 750$°C; $P_{CH_4} = 0.2$ bar; $CH_4/CO_2 = 1.0$; $W = 0.8$ g; $F = 380$ cm^3/min (ambient); $W/F = 4$ kg · s mol^{-1}. (a) Catalyst A; (b) catalyst B.

TABLE 2

Catalytic Performance of Ni/CaO–Al_2O_3 Catalysts in Reforming of CH_4 with CO_2 and Amount of Carbon Accumulated during 18 h on Stream ($T = 750$°C, $P_{CH_4} = 0.2$ bar, $P_{CO_2} = 0.2$ bar, $W/F_0 = 4$ kg · s mol^{-1})

Parameter	Catalyst A ($CaO/Al_2O_3 = 1/2$)	Catalyst B ($CaO/Al_2O_3 = 12/7$)
X_{CH_4} (%)	73	66
X_{CO_2} (%)	78	71
S_{CO} (%)	100	100
S_{H_2} (%)	97.5	98.0
Y_{H_2} (%)	71	64.7
Y_{CO} (%)	75.5	68.5
Carbon accumulated (wt%)	3.92	7.4

C. Characterization of Carbonaceous Species Studied by Transient Methods

The amounts and kinds of carbonaceous species formed during reforming reaction of methane with CO_2 at 750°C and at high CH_4 conversions, as well as their origin, CH_4 vs CO_2 molecule, were probed by TPH and TPO techniques as a function of catalyst support composition. In addition, transient isothermal hydrogenation experiments were conducted from which the intrinsic reactivity (intrinsic activation energy) of the hydrogenation process of these carbonaceous species as a function of catalyst support composition was estimated. The experimental results obtained from these studies are described below.

Temperature-programmed hydrogenation experiments. After reforming reaction at 750°C for time $\Delta t = 15$ min, the feed was changed to He for 5 min at 750°C, followed by cooling of the reactor to 300°C in He flow. The feed was then changed to pure H_2, while at the same time the temperature was increased to 750°C at the rate of 30°C/min to carry out a TPH experiment. Figures 4 and 5 show the CH_4 and C_2H_6 responses obtained during TPH with catalysts A and B, respectively. In both cases, the hydrogenation of carbonaceous species starts at about 500°C, and is complete at 750°C. In the case of catalyst A, a single CH_4 peak is obtained (Fig. 4), while in the case of catalyst B a distinct shoulder in the CH_4 response is formed isothermally at 750°C (Fig. 5). The CH_4 peak maximum appears at 655 and 700°C in the case of catalysts A and B, respectively, while the quantity of carbonaceous species hydrogenated

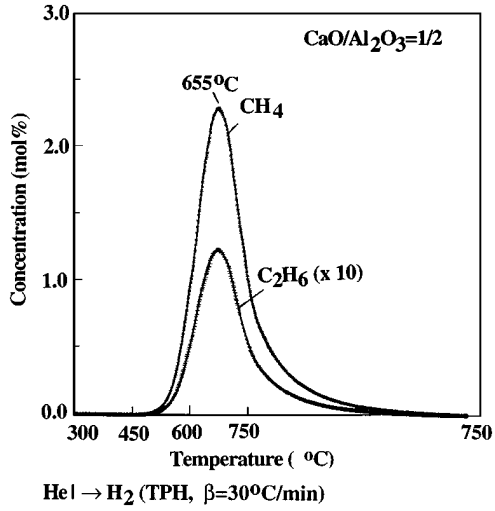

FIG. 4. Temperature-programmed hydrogenation (TPH) to CH_4 and C_2H_6 of carbon species formed during reforming reaction of CH_4 with CO_2 at 750°C over a 5 wt% Ni/CaO–Al_2O_3 (CaO/Al_2O_3 = 1/2) catalyst. Gas delivery sequence: CH_4/CO_2/He (750°C, 15 min) → He (750°C, 5 min) → cool in He flow to 300°C → H_2 (β = 30°C/min). W = 0.5 g; Q_{H_2} = 30 ml/min (ambient).

to CH_4 and C_2H_6 is found to be different in the two catalysts. In the case of catalyst A, the amounts of CH_4 and C_2H_6 produced are 318 and 17 μmol/g_{cat}, respectively, and in the case of catalyst B, 1357 and 72 μmol/g_{cat}, respectively. Of interest is the fact that the ratio of C_2H_6/CH_4 produced is approximately the same (0.05) over both catalysts. Similar experiments were performed for time on stream Δt = 2 h, and the results obtained are reported in Table 3.

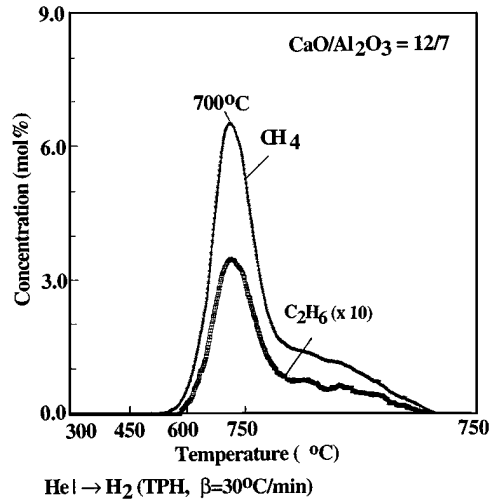

FIG. 5. Temperature-programmed hydrogenation (TPH) to CH_4 and C_2H_6 of carbon species formed during reforming reaction of CH_4 with CO_2 at 750°C over a 5 wt% Ni/CaO–Al_2O_3 (CaO/Al_2O_3 = 12/7) catalyst. Gas delivery sequence: CH_4/CO_2/He (750°C, 15 min) → He (750°C, 5 min) → cool in He flow to 300°C → H_2 (β = 30°C/min). W = 0.5 g; Q_{H_2} = 30 ml/min (ambient).

TABLE 3

Amounts of Carbonaceous Species Formed during Reforming Reaction of CH_4 with CO_2 Deduced by TPO and TPH Experiments (T = 750°C, P_{CH_4} = 0.2 bar, CH_4/CO_2 = 1, W/F = 23.2 kg · s mol^{-1})

	Carbon species (μmol/g)[a]			
	Catalyst A		Catalyst B	
Time on stream	TPO	TPH	TPO	TPH
5 min	470 (11.0)[b]	—[c]	410 (10.7)	—[c]
15 min	370 (8.7)	352	1600 (41.7)	1500
2 h	530 (12.4)	505	2450 (63.8)	2340
18 h	3265 (76.5)[d]	—[c]	6165 (161)[d]	—[c]

[a] Equivalent carbon deduced from CH_4 and C_2H_6 hydrogenation products or from the CO_2 oxidation product.

[b] Number in parentheses corresponds to equivalent monolayers of carbon (C/Ni_s = 1).

[c] Not measured.

[d] As determined by CHN analyzer; W/F = 4 kg · s mol^{-1}.

Noteworthy here is that accumulation of carbon species from a mixture of 20% CH_4/20% CO_2/He over both catalyst samples (Figs. 4 and 5) occurred with an appropriate W/F value so that similar CH_4 conversions were achieved (X_{CH_4} = 85–87% after 15 min of reaction). The CH_4 and CO_2 partial pressures at the end of the catalyst bed were, therefore, similar for both catalyst samples. Given the fact that the amount of sample used was the same in both experiments, the kind and amount of carbon accumulated has therefore been determined by the individual kinetics of carbon formation and removal operated over each catalyst surface exposed to given process variables.

Temperature-programmed oxidation experiments. The oxidation of carbonaceous species to CO_2, the former produced during reforming reaction at 750°C, was also used as a means to estimate their amount in comparison to that deduced via hydrogenation to CH_4 and C_2H_6 (Figs. 4 and 5). After reforming reaction for a given time, Δt, the feed was changed to He at 750°C for 5 min. At the end of this 5-min He purge of the catalyst, neither gaseous CO_2 nor CO was observed. The reactor was then cooled in He flow to 300°C, the feed was changed to a 10% O_2/He mixture, and the temperature was increased to 750°C at the rate of 30°C/min to carry out a TPO experiment. Figures 6a and b show CO_2 responses obtained during TPO in the case of catalyst A, following reforming reaction for time Δt = 15 min and 2 h, respectively. The oxidation of carbonaceous species starts at 450°C, while the CO_2 responses shown in Fig. 6 probe mainly for the presence of two kinds of carbonaceous species which exhibit different reactivity toward oxidation. Comparing the two CO_2 responses obtained with catalyst A, it is seen that by increasing the time of reaction from 15 min to 2 h the reactivity of carbonaceous species formed and their amount increase. More precisely,

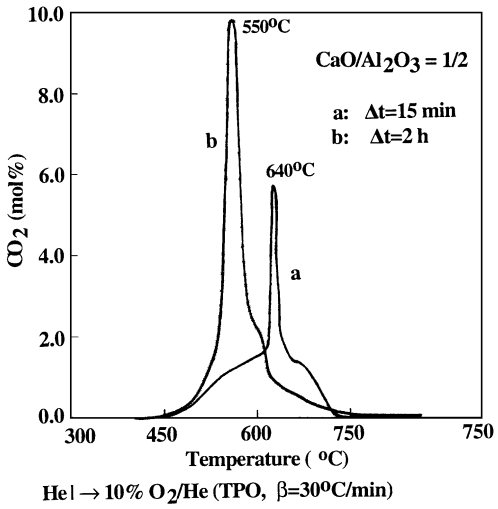

FIG. 6. Temperature-programmed oxidation (TPO) to CO_2 of carbon species formed during reforming reaction of CH_4 with CO_2 at 750°C over 5 wt% Ni/CaO–Al_2O_3 ($CaO/Al_2O_3 = 1/2$) catalyst. Gas delivery sequence: CH_4/CO_2/He (750°C, Δt) → He (750°C, 5 min) → cool in He flow to 300°C → 10% O_2/He ($\beta = 30$°C/min). $W = 0.5$ g; $Q_{O_2} = 30$ ml/min (ambient). (a) $\Delta t = 15$ min; (b) $\Delta t = 2$ h.

the distinct CO_2 peak maximum observed shifts to an appreciable extent, i.e., from 640 to 550°C, by increasing the reaction time from 15 min to 2 h, whereas the amounts of carbonaceous species formed are found to be 370 μmol/g_{cat} ($\theta_c = 8.7$) and 530 μmol/g_{cat} ($\theta_c = 12.4$) for $\Delta t = 15$ min and $\Delta t = 2$ h, respectively. The surface coverage, θ_c, is based on the Ni surface area, the latter determined by H_2 chemisorption (see previous section) and assuming also a ratio of one carbon atom per one Ni surface atom. The amounts of carbon species formed as a function of reaction time for both catalysts investigated are presented in Table 3. It should be noted that immeasurable amounts of CO and water were observed during all the TPO experiments performed. The absence of water strongly suggests that the carbonaceous species formed do not contain hydrogen. In addition, the 5-min He purge applied at 750°C before the TPO removes the adsorbed H_2O formed during reforming reaction.

The features of the TPO response curves shown in Fig. 6 and their interpretation (i.e., kinds of carbon species formed) must be considered carefully because of the high exothermicity of the combustion reaction and the relatively large quantities of carbon accumulated on the surface of the catalyst samples. The largest temperature rise in the catalyst bed expected for the conditions of the experiments presented in Fig. 6 can be estimated in the case in which the reactor is operated adiabatically. For a heat of combustion of 94 kcal/mol of carbon, based on its carbidic form (i.e., $C + O_2 \rightarrow CO_2$), the amount of carbon formed (530 μmol/g, Fig. 6b), and available data related to the thermal capacity of the $CaAl_2O_7$ compound (24), $\bar{c}_p = 0.25$ (cal/g K) in the range 450–750°C, the adiabatic temperature rise is estimated to be of the order of 200°C. In other words, if all carbon is burned instantly, and if all the heat released is absorbed by the catalyst sample, then the largest rise in temperature would be about 200°C. Such a result could be used to explain the relatively sharp increase in the rate of CO_2 formation observed in Figs. 6a (between 610 and 640°C) and 6b (between 530 and 580°C). However, in Figs. 9 and 10, where similar amounts of carbon have been accumulated as in Fig. 6, the CO_2 responses are rather broad and no sudden increase in the rate of CO_2 formation within a narrow temperature range is observed. In addition, no excursions in temperature (measured at the middle of the catalyst bed) were observed during the TPO experiments presented in Fig. 6. These remarks tend to suggest the following: (i) there are no significant temperature gradients within the catalyst particles under the nonadiabatic conditions of the TPO experiments, and (ii) the relatively sharp increase in the rate of CO_2 formation observed in Fig. 6 is rather due to the complex kinetics of the carbon combustion process which depends on the nature of carbon built as a function of reforming reaction time. The latter is discussed later. As shown in Table 3, in the case of catalyst B much larger quantities of carbon are accumulated between 15 min and 2 h on stream as compared with the case of catalyst A. Thus, the CO_2 responses obtained during TPO in the case of catalyst B are likely to have been influenced by the large exotherm of the combustion reaction and are, therefore, not presented for discussion.

Transient isothermal hydrogenation experiments. It has been shown in the literature (25) that transient isothermal hydrogenation of carbonaceous species (i.e., CH_x) to CH_4 at various temperatures results in CH_4 response curves certain features of which (i.e., time of appearance, t_m, of the CH_4 peak maximum) can be used to obtain intrinsic kinetic information on the hydrogenation process (i.e., number of rate-determining steps, activation energy). This methodology has been applied in the present work as described below.

After reforming reaction at 750°C for $\Delta t = 5$ min, the feed was changed to He at 750°C for 5 min, followed by cooling of the reactor under He flow to a certain temperature, T. The feed was then switched to H_2 to carry out isothermal hydrogenation of the carbonaceous species formed during reforming reaction. Figure 7 shows the CH_4 transient responses obtained at 600 and 700°C in the case of catalyst A, where the CH_4 peak maximum appears at $t_m = 1.28$ and 0.42 min, respectively. When the temperature of hydrogenation varies, it is seen that t_m also varies. This behavior is presented in Table 4 for both catalysts investigated. Based on kinetic models reported elsewhere (25), the results in Table 4 can be used to calculate the intrinsic activation energy of hydrogenation to CH_4 of the carbonaceous species formed under the present conditions investigated.

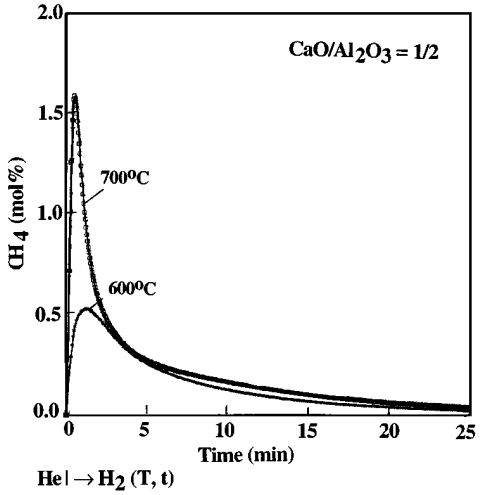

FIG. 7. Transient responses of CH_4 obtained during isothermal hydrogenation of carbonaceous species formed during reforming reaction over a 5 wt% Ni/CaO–Al_2O_3 ($CaO/Al_2O_3 = 1/2$) catalyst according to the gas delivery sequence: CH_4/CO_2/He (750°C, 5 min) → He (750°C, 5 min) → cool in He flow to $T \rightarrow H_2$ (T, t). $T = 600$ and 700°C.

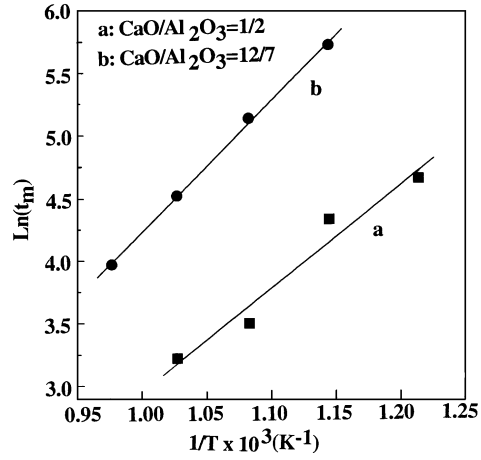

FIG. 8. Application of Eq. [1] of the model used to describe the kinetics of the isothermal hydrogenation of carbonaceous species formed during reforming reaction of CH_4 with CO_2 over 5 wt% Ni/CaO–Al_2O_3 catalysts. (a) $CaO/Al_2O_3 = 1/2$; (b) $CaO/Al_2O_3 = 12/7$.

The appropriate equation used is (25)

$$\ln(t_m) = \ln\left[\frac{\alpha - 1}{k_0 H}\right] + \left(\frac{E}{R}\right)\left(\frac{1}{T}\right), \qquad [1]$$

where α is the number of rate-determining steps of the hydrogenation process of equal k, H is the hydrogen surface concentration during hydrogenation (assumed constant), and $k = k_0 \exp(-E/RT)$. By plotting $\ln(t_m)$ versus $1/T$, a straight line is obtained, as shown in Fig. 8, the slope of which provides activation energies of 17 and 23 kcal/mol in the cases of catalysts A and B, respectively.

Origin of carbonaceous species formed during reforming reaction of CH_4 with CO_2 at 750°C. Isotopic experiments have been conducted (use of $^{13}CH_4$ in the feed) to probe for the relative contribution of the CO_2 and CH_4 reaction routes to accumulation of carbon species formed during reforming reaction at 750°C and at high CH_4 and CO_2 conversions. The experiment was as follows: After reforming reaction at 750°C for 5 min with a $^{13}CH_4$ (20%)/$^{12}CO_2$ (20%)/He mixture, the reactor was purged in He flow at 750°C for 5 min, followed by cooling to 300°C under He flow. The feed was subsequently switched to 10% O_2/He mixture, while at the same time the temperature was increased to 750°C at the rate of 30°C/min to carry out a TPO experiment. Of interest is the measurement of both $^{12}CO_2$ and $^{13}CO_2$ responses. It is noted that during the first 5 min of reforming reaction there was a drop in CH_4 conversion by 2–3 percentage units from the initial value ($t = 5$ s) of 85–88% obtained under the conditions of the experiments.

TABLE 4

Time of Appearance, t_m, of CH_4 Peak Maximum during Isothermal Hydrogenation of Carbonaceous Species Formed during CH_4/CO_2/He Reaction at 750°C

Catalyst 5 wt% Ni/	T (°C)	t_m (s)	E (kcal/mol)[a]
$CaO/Al_2O_3 = 12/7$	600	305	
	650	170	23
	700	92	
	750	53	
$CaO/Al_2O_3 = 1/2$	550	105	
	600	76	17
	650	33	
	700	25	

[a] Determined via Eq. [1].

Figures 9 and 10 show the $^{12}CO_2$ and $^{13}CO_2$ responses obtained during the TPO experiment described in the previous paragraph for catalysts A and B, respectively. In the case of catalyst A, the amounts of $^{12}CO_2$ and $^{13}CO_2$ produced are 325 and 152 μmol/g_{cat}, respectively ($^{12}CO_2/^{13}CO_2 = 2.14$); in the case of catalyst B (Fig. 10), the amounts of $^{12}CO_2$ and $^{13}CO_2$ are practically the same (205 μmol/g_{cat}, $^{12}CO_2/^{13}CO_2 = 1$). Also noted is the different shape of the CO_2 responses obtained with catalyst A (Fig. 9) as compared with catalyst B (Fig. 10). In the latter case, two kinds of carbon species could clearly be identified. These results demonstrate the effect of support composition on the relative rates of carbon formation and removal in the reaction routes of CH_4 and CO_2 to formation of CO. In addition, the effect of support on the kinds of carbon species formed is probed (different reactivity of carbon species toward oxidation to CO_2).

It is very important to clarify the fact that the second CO_2 peak observed in Figs. 9 and 10 during TPO experiments

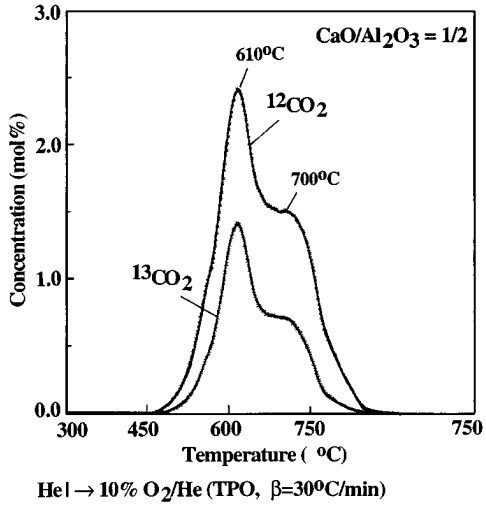

FIG. 9. Temperature-programmed oxidation (TPO) to $^{12}CO_2$ and $^{13}CO_2$ of carbon species formed during reforming reaction of $^{13}CH_4$ with $^{12}CO_2$ at 750°C over a 5 wt% Ni/CaO–Al_2O_3 (CaO/Al_2O_3 = 1/2) catalyst. Gas delivery sequence: $^{13}CH_4/^{12}CO_2$/He (750°C, 5 min) → He (750°C, 5 min) → cool in He flow to 300°C → 10% O_2/He ($\beta = 30$°C/min). $W = 0.5$ g; $Q_{O_2} = 30$ ml/min (ambient).

does not arise from the desorption of CO_2 which had been produced from the combustion of carbon at lower temperatures and remained adsorbed on the support surface. For this, CO_2 adsorption experiments followed by TPD had been conducted with the support material alone. It was found that for both support compositions used, the desorption of CO_2 is complete at 500°C, following adsorption at room temperature, and TPD under the same conditions as used in the TPO experiments (i.e., amount of sample, heating rate, and gas flow rate).

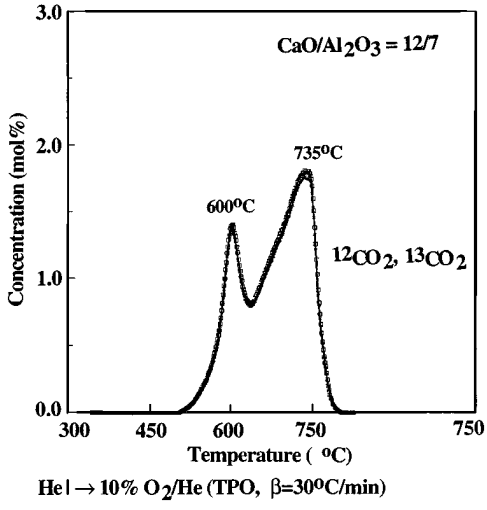

FIG. 10. Temperature-programmed oxidation (TPO) to $^{12}CO_2$ and $^{13}CO_2$ of carbon species formed during reforming reaction of $^{13}CH_4$ with $^{12}CO_2$ at 750°C over a 5 wt% Ni/CaO–Al_2O_3 (CaO/Al_2O_3 = 12/7) catalyst. Gas delivery sequence: $^{13}CH_4/^{12}CO_2$/He (750°C, 5 min) → He (750°C, 5 min) → cool in He flow to 300°C → 10% O_2/He ($\beta = 30$°C/min). $W = 0.5$ g; $Q_{O_2} = 30$ ml/min (ambient).

DISCUSSION

A. Catalytic Performance of Ni/CaO–Al_2O_3 Catalysts

Catalyst deactivation and resistance to coking are two important issues of the reforming reaction of methane with carbon dioxide over nickel-based catalysts for their potential industrial application. Thermodynamic calculations have been performed (3) which indicate that at temperatures higher than 950°C deposition of carbon via the reforming reaction of CH_4 with CO_2 can be avoided. However, lower reaction temperatures are desirable for industrial application. In addition, the use of CO_2/CH_4 feed ratios greater than unity leads to substantial reduction of carbon deposition (3).

Gadalla and Bower (3) have tested commercial Ni-based catalysts, used for steam reforming of CH_4, for their activity and stability during reforming of CH_4 with CO_2. Depending on support composition (γ-Al_2O_3, Al_2O_3–SiO_2, MgO–Al_2O_3, CaO–Al_2O_3) a different activity profile as a function of time on stream was obtained. A transient period of about 20 h was obtained before the continuously increased CH_4 conversion reached a stable level in the case of 12–14 wt% Ni supported on MgO–Al_2O_3 carrier. X-ray diffraction analysis of the calcined catalyst sample showed NiO, $MgAl_2O_4$, and α-Al_2O_3 as the main phases. Based on experimentally determined temperature profiles along the length of reaction zone as a function of reaction time, and also on XRD analyses, it was concluded (3) that in the case of Ni/MgO–Al_2O_3 catalyst endothermic reaction of Ni with excess α-Al_2O_3 to form the spinel structure of $NiAl_2O_4$ occurred simultaneously with the reforming reaction. It is to be noted that despite the loss of Ni sites to form the spinel solid solution no corresponding loss in activity was evidenced, a result suggesting that the new phase formed was more active than metallic nickel (3). In the case of 24–27 wt% Ni supported on CaO–Al_2O_3 (Al_2O_3/CaO = 4.6, molar ratio), XRD analyses of the catalyst sample before and after reaction indicated the existence of a new calcium aluminate phase, CA_2 (1 mol CaO : 2 mol Al_2O_3) but not of any $NiAl_2O_4$ (3).

Chen and Ren (12) have recently studied the effects of calcination temperature over a series of Al_2O_3-supported nickel catalysts on their activity and stability. At the low reaction temperature of 600°C, activity decreased with increasing calcination temperature (300–700°C), whereas at the high reaction temperature of 800°C, the differences in activity among these catalysts became smaller. Carbon deposition was found to decrease with increasing calcination temperature, while in the case of Ni/Al_2O_3 calcined at 800°C there was a continuous increase in activity up to 1.5 h

on stream. The above-mentioned observations, along with XRD and XPS measurements, suggested that the calcined $NiAl_2O_4$ spinel phase formed is not active in reforming reaction, but its reduced form can lead to significant activity and stability.

The present 5 wt% Ni/CaO–Al_2O_3 catalysts exhibit very stable catalytic performance for reforming reaction times between 1 and 18 h on stream and at a reaction temperature ($T = 750°C$) convenient for industrial practice. On the other hand, during the first 1 h of operation some deactivation takes place. As expected, under the reaction conditions investigated ($T = 750°C$, $CH_4/CO_2 = 1.0$) carbon deposition is predicted by thermodynamics. However, the amount of accumulated carbon with time on stream (see Table 3) did not affect the high activity of the catalyst (Fig. 3) after 1 h on stream. Based on the previous discussion related to the activity behavior observed over various nickel-based catalysts (3, 12), it can be suggested that for the present catalytic systems, no crystal phase transformations in support composition and/or creation of Ni sites during reaction occurred. This is due to the fact that a high calcination temperature was used for the preparation of supports ($T_c = 1100°C$), before deposition of Ni had taken place, and also after catalyst preparation ($T_c = 900°C$), preventing, therefore, any further solid-state reactions to take place under favorable reaction conditions. In the case of catalyst B (see Table 1), only one calcium aluminate spinel structure is formed (at least detected by XRD), where NiO is the only nickel-containing compound formed after catalyst calcination at 900°C. As discussed later, this NiO phase can all essentially by reduced to metallic Ni^0 following H_2 reduction at 750°C for 2 h. In the case of catalyst A, calcination of the fresh sample at 900°C for 10 h resulted in a small amount of $NiAl_2O_4$ according to XRD (Table 1), H_2 TPR (Fig. 1), and H_2 TPD (Fig. 2) measurements to be discussed later. According to the literature (26), the $NiAl_2O_4$ cannot be reduced in H_2 at 750°C. Thus, in the present case possible formation of new active Ni sites by some interaction of the nickel metal surface and support during reaction conditions must be excluded.

Zhang and Verykios (10) and Yamazaki *et al.* (7) found that addition of CaO on 17 wt% Ni/γ-Al_2O_3 ($CaO/Al_2O_3 = 10$), calcined at 750°C and reduced in H_2 at 750°C, and on Ni/MgO–CaO catalyst ($Ni_{0.03}Ca_{0.13}Mg_{0.84}O$), calcined at 950°C for 20 h and reduced in H_2 at 850°C, resulted in very stable catalytic systems after 1–2 h of reforming reaction of CH_4 with CO_2 in the temperature range 750–850°C. In the case of Ni/CaO–Al_2O_3 catalyst (10), it was suggested that despite the larger amount of carbon accumulated as compared with Ni/γ-Al_2O_3, the improved stability exhibited by the former catalyst could be attributed to the more reactive form of carbon produced as compared with that formed with the Ni/γ-Al_2O_3 system. On the other hand, for the Ni/MgO–CaO system (7), it was suggested that the smaller amount of carbon formed as compared with the Ni/MgO catalytic system could be due to the higher basicity induced by the added amount of CaO which is expected to enhance adsorption of CO_2. This, in turn, could promote the reverse Boudouard reaction, $CO_2 + C \leftrightharpoons 2CO$, thus lowering the amount of accumulated carbon.

In this work, the small deactivation of the 5 wt% Ni/CaO–Al_2O_3 catalysts found during the first 1 h of reaction must only be due to the accumulation of carbonaceous species on the active catalyst surface (see Table 3), in relation to what was mentioned in the previous paragraphs. The very good stability exhibited by the present catalysts after 1 h on stream and for 18 h of reaction, despite the significant amount of carbon deposition, must mainly be related to its site location and the extent by which this carbon participates as an active intermediate species in the reforming reaction. The results in Table 3 correspond to the total amount of carbon accumulated on the catalyst surface after a given reaction time. Part of this carbon is a true reaction intermediate species, the amount of which can be determined only by steady-state tracing experiments, as has recently been demonstrated by Efstathiou *et al.* (27) in the case of supported Rh catalysts. Aspects of the site location and characterization of the carbon species as a function of catalyst support composition are discussed in the next section.

The lower steady-state activity obtained with catalyst B as compared with catalyst A (Fig. 3) could be ascribed mainly to two reasons: First, a larger amount of carbon is accumulated on catalyst B than on catalyst A (see Table 3), a result that can reduce the available nickel-active surface area; it is noted that both catalysts have a similar initial (before reaction) nickel surface area according to the H_2 chemisorption results of Fig. 2. Second, the reforming reaction of CH_4 with CO_2 could be considered as a structure-sensitive reaction over nickel-supported catalysts. As discussed in the next section, the results in Figs. 1, 2, 9, and 10 support the existence of a nickel particle size distribution in the present catalyst formulations. It can only be speculated whether the small amount of $NiAl_2O_4$ compound found in catalyst A could significantly contribute to its higher activity as compared with that of catalyst B.

B. Characterization of Carbon Species Formed during Reforming of CH_4 with CO_2

The formation of carbon during the reforming reaction of CH_4 with CO_2, based on the isotopic results of the present work and those in the literature (13, 14, 18, 27–30), is suggested to be due to the following elementary reaction steps:

$$CH_4(s) \rightarrow CH_x(s) + (4 - x)H(s), \quad [2]$$

$$CH_x(s) \rightarrow C(s) + xH(s), \quad [3]$$

$$CO_2(g) \leftrightharpoons CO(s) + O(s), \quad [4]$$

$$CO(s) \leftrightharpoons C(s) + O(s), \quad [5]$$

where (s) is a site on the reduced nickel surface. Removal of carbon from the surface could take place by the elementary reaction step

$$C(s) + OH(s) \leftrightharpoons CO(s) + H(s) \quad [6]$$

in addition to the backward step of reaction [5] (this step is part of the reaction $CO_2 + C \rightarrow 2CO$). The OH(s) surface species are derived from the dissociation of adsorbed H_2O on the nickel surface. It should be noted here that some of the above-mentioned reaction steps, [2]–[6], could also take place to a small extent over the present support compositions. In fact, slight catalytic activity was observed under the conditions of the experiments presented in Fig. 3 ($X_{CH_4} < 3\%$). In addition, the transformation of adsorbed atomic carbon shown in reaction steps [2]–[6] to another form is discussed later.

The isotopic TPO experiments presented in Figs. 9 and 10 allowed us to quantitatively determine the carbon accumulation derived from the CH_4 and CO_2 molecules, after a given time on stream and similar levels of high CH_4 and CO_2 conversions over the two Ni/CaO–Al_2O_3 catalysts investigated. These results have also demonstrated the effects of support composition (CaO/Al_2O_3 ratio) on the kinds of carbon species formed and their reactivities toward oxidation. For both catalyst formulations, two kinds of carbon species could be identified. After 5 min of reforming reaction at 750°C, there is a larger amount of carbon derived from CO_2 on the surface of catalyst A than catalyst B, whereas there is a large amount of carbon derived from CH_4 on the surface of catalyst B than catalyst A; note that the numbers of Ni-exposed surface sites per gram of catalyst, as determined by H_2 chemisorption, are practically the same for both catalysts. These results can be explained based on the following remarks.

It has been reported (31–34) that dissociation of CO (reaction step [5]) involves ensembles of Ni atoms as active sites, the number of which is in the range 4 to 6. The density of these ensembles increases with increasing metal particle size (35). On the other hand, studies on Ni single crystals suggest that the more open nickel surface is the most active for CH_4 dissociation, while the close-packed nickel surface is the least active (36). More open metal surfaces can be obtained by decreasing the metal particle size of a metal-supported catalyst. The above-mentioned observations for methane decomposition (reaction steps [2] and [3]) and CO dissociation (reaction step [5]) over Ni surfaces can explain the results in Figs. 9 and 10 if it is considered that the two catalysts exhibit different nickel particle morphologies. More precisely, the nickel surface of catalyst B is expected to consist of a larger fraction of nickel particles of smaller size than those of catalyst A.

The assumed different morphologies of Ni particles in the two catalytic systems are supported by both H_2 TPR (Fig. 1) and H_2 TPD (Fig. 2) results. The H_2 TPR results in Fig. 1, following calcination at 750°C for 1 h, show two important features. The first one is that more than 95% of the total nickel present in the sample (5 wt%) can be reduced to Ni^0 according to the reaction

$$NiO + H_2 \rightarrow Ni^0 + H_2O. \quad [7]$$

The second feature is that the amount of H_2 consumed in the range 300–500°C in the case of catalyst A is about twice that of catalyst B (see Fig. 1). It is expected that reduction of small NiO particles, chemically bound on the support surface, would be more difficult than the reduction of large particles. Therefore, the H_2 TPR results in the range 300–500°C (Fig. 1) suggest that catalyst A consists of a large fraction of NiO particles of large mean diameter than catalyst B. Also, given the fact that the total number of nickel surface-exposed atoms is about the same in both catalysts (Fig. 2), it is concluded that the fraction of NiO particles of small diameter is larger in the case of catalyst B than of catalyst A. Of course, the present H_2 TPR results cannot be used to quantify the Ni particle size distribution they imply.

Three hydrogen desorption peaks were identified under the stated experimental conditions for both catalysts. However, large differences in the amounts of H_2 desorbed at temperatures in the ranges 50–500 and 500–750°C are seen. Thus, there must exist a different distribution in the concentration of each of the kinds of Ni sites mentioned in the previous paragraph for the same total number of exposed surface nickel atoms in both catalyst samples. As discussed in Section C in more detail, the high-temperature H_2 desorption peak observed on catalyst B ($T_M = 540$°C) is likely due to some electronic modifications of the smaller nickel crystallites ($d < 10$ nm) which interact intimately with the calcium aluminate support.

Carbon chemical and morphological structure. There is yet very little information published related to the chemical structure of carbon species deposited on nickel-based catalysts during reforming reaction of CH_4 with CO_2 (12, 13). Chen and Ren (12) have used TEM to directly observe the growth of filamentous carbon during reforming reaction over alumina-supported nickel catalysts, where Ni particles have also been observed on the tip of this filamentous carbon. In a recent work, Swaan *et al.* (13) conducted isotopic TPO experiments similar to those presented in Figs. 9 and 10 over a 4 wt% Ni/SiO_2 catalyst following reforming reaction ($T = 700$°C, $P_{CH_4} = 0.075$ bar, $CO_2/CH_4 = 2$, $P_T = 1$ bar). Two CO_2 peaks were identified, the first with a peak maximum at $T_{M_1} = 500$°C and the second (a broad one) at $T_{M_2} = 650$°C. The proportion of carbon originating from CO_2 as opposed to CH_4 was found to be about 1.5, a result similar to that obtained in the present work. Based on magnetic measurements, it was shown that both kinds of carbon did not affect significantly the ferromagnetic signal, a result that discards any hypothesis of bulk nickel carbide

or interstitial carbon formation. Tracer experiments have indicated that the first kind of carbon (oxidized at low temperatures) originates mostly from methane dissociation and accumulates preferentially during the early period of reaction. It was suggested that this carbon might be of the Ni_3C form (13). Due to the low content and dispersion of nickel used (13), no clear detection of such a carbide phase could be obtained by magnetic measurements. The second type of carbon was much more stable toward oxidation, and its accumulation closely followed the rate of catalyst deactivation. It was suggested (13) that this carbon could progressively encapsulate the nickel particles without interacting chemically with nickel, thereby causing the deactivation observed. In addition, this carbon was suggested to arise from the Boudouard reaction, $2CO \leftrightharpoons C + CO_2$, based on isotopic transient experiments (13).

In this work, no direct evidence is reported for the chemical structure and morphology of carbon accumulated over the $Ni/CaO–Al_2O_3$ catalysts. However, the TPO experiments presented in Figs. 6, 9, and 10 demonstrate the existence of mainly two kinds of carbon species, free of chemically bound hydrogen (no H_2O was obtained during TPO), the origin of which (CH_4 vs CO_2 molecule) depends on support composition in a manner explained in detail in previous paragraphs. The chemical and morphological nature of these carbon species can only be suggested based on the following.

The large amount of carbon accumulated with reaction time (Table 3) and the excellent stability exhibited by the catalysts during the reaction period of 1–18 h clearly imply that this carbon cannot be all of carbidic form, either as adsorbed atomic or Ni_3C. Taking into account the literature results concerning the characterization of carbon formed during reforming reaction over Ni/Al_2O_3 (12) and Ni/SiO_2 (13) catalysts, which have already been discussed, and previous work on the nature of carbon formed during methane-steam reforming over nickel-based catalysts (18, 37), it is suggested that after 5 min of reforming reaction the high-temperature peak of CO_2 shown in Figs. 9 and 10 could be assigned to amorphous and/or graphite forms of carbon. Whether all of this carbon resides on the surface of nickel particles or some of it is transferred onto the support surface cannot be answered from the results of the present work. The second kind of carbon species oxidized at lower temperatures (see Figs. 9 and 10) is suggested to be of filamentous form. This assignment is supported by the proposed mechanism of its formation (1, 38) and the TPO results in Figs. 6 and 9. According to kinetic results reported in the literature (39), adsorbed carbon atoms (derived from CH_4 decomposition and CO dissociation) can be transformed to either a polymeric or filamentous form. Adsorbed carbon atoms can first dissolve in the nickel crystallites, then diffuse through the metal followed by precipitation at the rear of the nickel particle to form a polymeric carbon filament. Thus, the nickel particle can be lifted off the support moving outward on top of the growing filament (1, 38). Such a process can explain both the large amounts of carbon built up on the catalyst surface and the catalyst stability with high activity for long times on stream (Fig. 3). By comparing the TPO results of Figs. 6 and 9, it is seen that there is continuous growth of the low-oxidation-temperature CO_2 peak(s) and a decrease in the high-temperature CO_2 peak. In addition, the amount of carbon formed after 15 min of reaction is found to be smaller than that corresponding to 5 min of reaction (see Table 3, catalyst A). These results support the mechanism of filamentous carbon formation and may be also point out that during reaction some transformation of carbon occurs between the main two carbon forms.

The amounts of carbon accumulated during the reaction period of 15–120 min on stream given in Table 3 (corresponding to the same *W/F* value) result in different average rates of carbon accumulation over the two catalysts investigated. In the case of catalyst A, the rate of carbon accumulation is found to be 1.52 μmol/g · min, compared with the value of 8.1 μmol/g · min obtained in the case of catalyst B. In addition, it is found that for catalyst A the amount of carbon accumulated during 15 min on stream is slightly lower than the amount obtained during the first 5 min of reaction, whereas the opposite is true for catalyst B (see Table 3). These results indicate that the rates of carbon formation and removal depend on time on stream and catalyst surface composition. As shown in Table 2 and Fig. 3, the process conditions during the first 2 h of reaction are different for the two catalysts. It has been reported (18) that in the case of steam reforming of methane over nickel-based catalysts, the rate of poisoning of the nickel surface by carbon depends on the particular H_2O/C ratio. It is believed that this parameter also plays an important role in carbon deposition in the present work. In addition, as previously discussed, formation of filamentous carbon can be associated with dissolution of carbon into the bulk of nickel crystallites. The kinetics of this process may be influenced by the size and morphology of nickel particles, parameters that are different for the present two catalysts as extensively discussed in previous paragraphs.

It has recently been shown that in the case of reforming reaction over a Rh/Al_2O_3 catalyst in the range 650–750°C (28, 29), carbon accumulated on the catalyst surface is derived mainly from the CO_2 molecule, a result different from that observed in this work and reported by Swaan *et al.* (13). These results demonstrate the different kinetics of carbon formation and removal steps occurring during reforming reaction of CH_4 with CO_2 over supported Rh and Ni surfaces. It could be suggested that reaction steps found in the sequence from CH_4 to CO formation are faster over the Rh than the Ni surface during reforming reaction.

As mentioned under Results, despite the large adiabatic temperature rise estimated for the conditions of the

experiments presented in Figs. 6, 9, and 10, it is argued that the relatively sharp CO_2 peaks in Figs. 6, but not in Figs. 9 and 10, may be due to intrinsic kinetic reasons associated with the combustion process of the kind (i.e., structure and morphology) of carbon species formed during a given time on stream. According to the discussion offered in the previous paragraphs, the growth of filamentous carbon appears to be governed by a complex kinetic process. Also, the fact that in the present catalysts a nickel particle size distribution seems to exist, as discussed previously, adds another parameter that may control the structure and morphology of filamentous carbon formed. One explanation for the sharp CO_2 peaks in Fig. 6 might be the sudden increase in the concentration of carbon atoms exposed to the oxygen gas atmosphere during the disintegration of polymeric and filamentous carbon, or even of some Ni_3C, by the combustion process. According to mathematical analysis of the TPH of carbon species to methane reported by Bianchi and Gas (40), the temperature at which the maximum rate occurs, T_M, depends on the following kinetic parameters: (i) the intrinsic activation energy of the hydrogenation process, (ii) the preexponential factor, (iii) the heat of hydrogen adsorption, and (iv) the concentration of sites for H_2 chemisorption at T_M. The first two parameters are associated with the chemical step that controls the overall hydrogenation process. Thus, it is reasonable to argue that similar kinetic parameters may influence T_M during TPO. In the case of Fig. 6, as time on stream increases from 15 min to 2 h, the structure and morphology of polymeric and filamentous carbon could change, giving rise to a shift in the T_M of CO_2 formation during combustion.

Hydrogenation of carbon species. The reactivity of carbon species toward hydrogenation as a function of the present catalyst support composition has been studied, and a kinetic analysis of this hydrogenation process performed (see Figs. 7 and 8). According to this analysis (25), stepwise addition of hydrogen atoms to the carbon atoms to form CH_4 is assumed to be the prevailing mechanism. Hydrogen atoms are formed on the metal surface via a dissociation step of gaseous H_2. In the present work, as extensively discussed in previous paragraphs, it is suggested that a large part of the carbon deposited on the catalyst surface is of the filamentous form. The results also suggest that a significant amount of nickel could be found on top of these carbon filaments. Taking into account these remarks, hydrogenation of this carbon form must also be associated with C–C bond breaking. According to the good fit of the data in Fig. 7 to the kinetic model used (25, Eq. [1]), it appears that the C–C bond breaking step may not influence significantly the overall rate of the hydrogenation process. In addition, surface diffusion of hydrogen atoms toward the interface between the nickel particles and carbon filaments may also not control the hydrogenation process. The higher activation energy of hydrogenation of carbon obtained in the case of catalyst B as compared with catalyst A (see Table 4), according to the kinetic analysis used, is also consistent with the results of TPH (see Figs. 4 and 5) and TPO (see Figs. 9 and 10) experiments.

In the case of oxidation of carbon to CO_2 (Figs. 6, 9, and 10), there has not been reported in the literature a detailed kinetic model that describes the TPO process of filamentous carbon, on top of which nickel particles are found. It is suggested that a mechanism similar to that discussed for the hydrogenation process might apply according to the elementary steps

$$O_2 + 2(s) \underset{k_{-1}}{\overset{k_1}{\rightleftharpoons}} 2O(s), \qquad [8]$$

$$C + O(s) \xrightarrow{k_2} CO(s), \qquad [9]$$

$$CO(s) + O(s) \xrightarrow{k_3} CO_2 + 2(s), \qquad [10]$$

where (s) is a site on the nickel surface. Steps such as the C–C bond breaking and surface diffusion of adsorbed oxygen and carbon atoms to form CO could also be considered to influence the rate of combustion of filamentous carbon. As already mentioned in a previous paragraph, the features of the TPO responses observed in Fig. 6 may be related to the aforementioned remarks. It has recently been shown by Tsipouriari *et al.* (41) that reaction steps [9] and [10] could both be considered rate-limiting steps in the case of carbon oxidation to CO_2 over Rh/Al_2O_3 catalyst, the carbon being produced under CO_2 reforming reaction conditions at 650°C. This result was derived based on transient isothermal oxidation experiments performed similarly to those in the present work (Fig. 7) for the case of carbon hydrogenation to CH_4 and also on a kinetic analysis (41). Similar experiments could be conducted for the present Ni-supported catalysts, but a kinetic analysis of the transient CO_2 response must likely account for aspects related to other mechanistic steps as outlined previously. This was out of the scope of the present investigation.

The observation that the appearance of the CH_4 peak maximum with time on stream can be shifted by varying the hydrogenation temperature (see Fig. 7) is explained by the fact that more than one step with similar rate constant, k, control the rate of the hydrogenation process (25). On the other hand, hydrogenation of carbon accumulated over a Rh/Al_2O_3 catalyst after 10 min of reforming reaction at 650°C, and for the same feed gas composition used in the present work, proceeds with an activation energy of 30 kcal/mol, while only one rate-determining step for the hydrogenation process was evident; no shift in the t_m with T has been observed (41) as opposed to the present case (Fig. 7). As previously discussed, the support composition of the present catalysts has affected the morphology of Ni particles, and as a result, different kinds of carbon, with respect to their structure and reactivity toward oxidation and hydrogenation, were formed during reforming reaction.

In situ FT-IR measurements obtained after 10 min of reforming reaction of CH_4 with CO_2 at 700°C have indicated no adsorbed carbonate-like species over catalyst A ($CaO/Al_2O_3 = 1/2$), and only a very weak IR band at 1450 cm^{-1} (assigned to ionic carbonate species) was obtained over catalyst B ($CaO/Al_2O_3 = 12/7$). Therefore, the CH_4 and C_2H_6 responses obtained during temperature-programmed and isothermal hydrogenation experiments presented in Figs. 4, 5, and 7 are not partly due to any hydrogenation process of carbonate species. In fact, the 10-min He purge applied at 750°C, after the reforming reaction and before the hydrogenation process, removes the small amounts of CO_3^{2-} on the surface of catalyst B via decomposition reaction to CO_2.

The removal of carbon by the reverse Boudouard reaction of adsorbed CO_2 species on the support can be ruled out in the present work according to what was mentioned in the previous paragraph. It is noted that more carbon is accumulated after 18 h of reaction at 750°C over catalyst B than catalyst A (see Table 3), where the former catalyst was found to adsorb some CO_2. On the other hand, it is noted that the same reaction can proceed on the Ni surface.

C. H_2 Chemisorption over Ni/CaO–Al_2O_3 Catalysts

The H_2 TPD response obtained in the present work with 5 wt% Ni/CaO–Al_2O_3 ($CaO/Al_2O_3 = 1/2$, Fig. 2a) catalyst shows features similar to those reported by Weatherbee and Bartholomew (42) in the case of 14 wt% Ni/Al_2O_3 catalyst. However, the high-temperature H_2 desorption peak ($T_M = 540$°C) observed over the present 5 wt% Ni/CaO–Al_2O_3 ($CaO/Al_2O_3 = 12/7$, Fig. 2b) catalyst has not been previously reported, to our knowledge, over supported Ni catalysts with common support compositions (i.e., SiO_2, Al_2O_3, TiO_2). High-temperature hydrogen desorption states ($T_M = 300$–450°C) observed over Ni/Al_2O_3 and Ni/TiO_2 have been suggested to arise from some electronic modifications of small nickel crystallites which interact intimately with the support (42, 43). This explanation is also adopted in the present work. The present XPS results have indicated a higher surface concentration of oxygen in the case of $Ca_{12}Al_{14}O_{33}$ spinel structure support (catalyst B) than in the case of catalyst A with a support composition consisting of $NiAl_2O_4$, $CaAl_4$, O_7, and $CaAl_2O_4$ phases. During impregnation the same amount of Ni^{2+} ions are, therefore, expected to interact with more oxygen species in the case of catalyst B than of catalyst A, while the strength of this interaction must be proportional to the effective surface charge of the oxygen ions in the two support compositions. After calcination of the catalysts at 900°C, it seems that stronger interactions of Ni^{2+} with O^{n-} species of support in the case of catalyst B are developed, which are expected to reduce the fraction of NiO crystallites with large diameter as compared with the case of catalyst A.

CONCLUSIONS

The following conclusions can be drawn from the present investigation:

1. Five weight percent nickel supported on spinel calcium aluminate phases ($CaAl_4O_7$, $CaAl_2O_4$, and $Ca_{12}Al_{14}O_{33}$) results in a very active and stable catalytic system for the reforming reaction of CH_4 with CO_2 ($P_{CH_4} = 0.2$ bar, $CH_4/CO_2 = 1$) at 750°C over 18 h of testing. A small drop in activity, but not in CO and H_2 selectivity, is observed during the first hour of reaction.

2. The carbonaceous species accumulated during reaction at 750°C are found to be free of chemically bound hydrogen, where their origin, CH_4 versus CO_2 molecule, and their reactivities toward oxidation and hydrogenation are found to strongly depend on support composition (molar ratio of CaO to Al_2O_3). This is the result of the effects of support composition on the morphology and particle size distribution of nickel metal.

3. Reforming reaction of CH_4 with CO_2 at 750°C over 5 wt% Ni/CaO–Al_2O_3 ($CaO/Al_2O_3 = 1/2$ and 12/7) catalysts results mainly in two kinds of carbon species. Hydrogenation of carbon species formed during 5 min of reforming reaction proceeds with activation energies of 17 and 23 kcal/mol in the case of $CaO/Al_2O_3 = 1/2$ and 12/7 support compositions, respectively.

4. Calcination of 5 wt% Ni/CaO–Al_2O_3 ($CaO/Al_2O_3 = 12/7$) with 10% O_2/He at 750°C results in the conversion of all nickel to nickel oxide, where the latter compound can be reduced in pure H_2 at 750°C to an extent greater than 95%.

5. H_2 chemisorption over a 5 wt% Ni/CaO–Al_2O_3 ($CaO/Al_2O_3 = 12/7$) catalyst results in an unusually high temperature TPD peak ($T_M = 540$°C). It is suggested that this behavior is the result of some strong electronic interactions of small nickel crystallites with the $Ca_{12}Al_{14}O_{33}$ support.

ACKNOWLEDGMENTS

This work was supported by the Commission of the European Community (Contract JOU2-CT92-0073). Dr. W. Grünert (Ruhr Universität, Bochum, Germany) is acknowledged for his help with the XPS measurements.

REFERENCES

1. Trimm, D. L., *Catal. Rev. Sci. Eng.* **16**, 155 (1977).
2. Rostrup-Nielsen, J. R., *in* "Catalysis Science and Technology" (J. R. Anderson and M. Boudart, Eds.), Vol. 5. Springer, New York, 1984.
3. Gadalla, A. M., and Bower, B., *Chem. Eng. Sci.* **43**, 3049 (1988).
4. Rostrup-Nielsen, J. R., and Bak Hasen, J.-H., *J. Catal.* **144**, 38 (1993).
5. Richardson, J. T., and Paripatyadar, S. A., *Appl. Catal.* **61**, 293 (1990).
6. Ashcroft, A. T., Cheetman, A. K., Green, M. L. H., and Vernon, P. D. F., *Nature* **352**, 225 (1991).
7. Yamazaki, O., Nozaki, T., Omata, K., and Fujimoto, K., *Chem. Lett.,* 1953 (1992).

8. Erdöhelyi, A., Cserenyi, J., and Solymosi, F., *J. Catal.* **141**, 287 (1993).
9. Zhang, Z. L., and Verykios, X. E., *J. Chem. Soc. Chem. Commun.,* 71 (1995).
10. Zhang, Z. L., and Verykios, X. E., *Catal. Today* **21**, 589 (1994).
11. Gadalla, A. M., and Sommer, M. E., *Chem. Eng. Sci.* **44**, 2825 (1989).
12. Chen, Y.-G., and Ren, J., *Catal. Lett.* **29**, 39 (1994).
13. Swaan, H. M., Kroll, V. C. H., Martin, G. A., and Mirodatos, C., *Catal. Today* **21**, 571 (1994).
14. Osaki, T., Masuda, H., and Mori, T., *Catal. Lett.* **29**, 33 (1994).
15. Ruckenstein, E., and Hu, Y. H., *Appl. Catal. A* **133**, 149 (1995).
16. Sodesawa, T., Dobashi, A., and Nozaki, F., *React. Kinet. Catal. Lett.* **12**, 107 (1979).
17. Chubb, T. A., *Sol. Energy* **24**, 341 (1980).
18. Bartholomew, C. H., *Catal. Rev. Sci. Eng.* **24**, 67 (1982).
19. Lemonidou, A. A., and Vasalos, I. A., *Appl. Catal.* **54**, 119 (1989).
20. Efstathiou, A. M., Papageorgiou, D., and Verykios, X. E., *J. Catal.* **141**, 612 (1993).
21. Briggs, D., and Seah, M. P., "Practical Surface Analysis," 2nd ed., Vol. 1. Wiley, New York, 1990.
22. Shalvoy, R. B., and Reucroft, P. J., *J. Catal.* **56**, 336 (1979).
23. Ng, K. T., and Hercules, D. M., *J. Phys. Chem.* **80**, 2094 (1976).
24. Kubaschewski, O., and Alcock, C. B. (Eds.), "Metallurgical Thermochemistry." Pergamon, Elmsford, NY.
25. Bianchi, D., and Gass, J. L., *J. Catal.* **123**, 298 (1990).
26. Scheffer, B., Molhoek, P., and Moulijn, J. A., *Appl. Catal.* **46**, 11 (1989).
27. Efstathiou, A. M., Kladi, A., Tsipouriari, V., and Verykios, X. E., *J. Catal.* **158**, 64 (1996).
28. Tsipouriari, V. A., Efstathiou, A. M., Zhang, Z. L., and Verykios, X. E., *Catal. Today* **21**, 579 (1994).
29. Zhang, Z. L., Tsipouriari, V., Efstathiou, A. M., and Verykios, X. E., *J. Catal.* **158**, 51 (1996).
30. Turlier, P., Pereira, E. B., and Martin, G. A., *in* "Proceedings, International Conference on Carbon Dioxide Utilization, Bari, Italy, 1993," p. 119.
31. Rostrup-Nielsen, J. R., *J. Catal.* **27**, 343 (1972).
32. Van Dijk, W. L., Groenewegen, J. A., and Ponec, V., *J. Catal.* **45**, 272 (1976).
33. Martin, G. H., Primet, M., and Dalmon, J. A., *J. Catal.* **53**, 321 (1978).
34. Kuijpers, E. G. M., Kock, A. J. H. M., Nieuwesteeg, M. W. C. M. A., and Geus, J. W., *J. Catal.* **95**, 13 (1985).
35. Che, M., and Bennett, C. O., *in* "Advances in Catalysis" (D. D. Eley, H. Pines, and P. B. Weisz, Eds.), Vol. 36, pp. 55–172. Academic Press, San Diego, 1989.
36. Beebe, T. P., Jr., Goodman, D. W., Key, B. D., and Yates, J. T., Jr., *J. Chem. Phys.* **87**, 2305 (1987).
37. Deken, J. D., Menon, P. G., Froment, G. F., and Haemers, G., *J. Catal.* **70**, 225 (1981), and references therein.
38. Baker, R. T. K., and Harris, P. S., *in* "Chemistry and Physics of Carbon" (P. L. Walker, Jr., Ed.), Vol. 14, p. 83. Dekker, New York, 1979.
39. McCarty, J. G., and Wise, H., *J. Catal.* **57**, 406 (1979).
40. Bianchi, D., and Gass, J. L., *J. Catal.* **123**, 310 (1990).
41. Tsipouriari, V. A., Efstathiou, A. M., and Verykios, X. E., *J. Catal.* **160**, 31 (1996).
42. Weatherbee, G. D., and Bartholomew, C. H., *J. Catal.* **87**, 55 (1984).
43. KaO, C.-C., Tsai, S.-C., and Chung, Y.-W., *J. Catal.* **73**, 136 (1982).